Journal of Mineralogical and Petrological Sciences, Volume 97, page 137-143, 2002 Sueno Issue

Crystal structures and infrared spectra of two Fe-bearing hydrous magnesium silicates synthesized at high temperature and pressure

Hexiong YANG*, Charles T. PREWITT**, and Zhenxian LIU**

*Jet Propulsion Laboratory, M/S 183-301, 4800 Oak Grove Drive, Pasadena, CA 91109-8099, U.S.A.
**Geophysical Laboratory, Carnegie Institution of Washington, 5251 Broad Branch Rd. NW, Washington DC 20015-1305, U.S.A.

Two Fe-bearing hydrous magnesium silicates, Fe-bearing phase E with the composition $Mg_{2.22}Fe_{0.52}Si_{0.98}O_6H_{2.08}$, and phase E' with the composition $Mg_{2.13}Fe_{0.59}Si_{0.87}O_6H_{2.52}$, were synthesized at 14 GPa and 1000 °C and studied with single-crystal X-ray diffraction and infrared spectroscopy. The space groups and unit-cell parameters are $R\bar{3}m$, a = 2.981(1) Å, c = 13.898(3) Å for Fe-bearing phase E, and $P6_3/mmc$, a = 2.953(1) Å, c = 14.170(1) Å for phase E'. In addition to the similar compositions and unit-cell parameters, phase E' possesses many structural features characteristic of those of Fe-bearing phase E. Most remarkably, both structures are built of close-packed oxygen atoms along the c axis, with all Si occupying the interstitial tetrahedral sites and M (= Mg + Fe) cations occupying the octahedral sites. All cation sites are partially occupied in both structures. The implausible configuration of M octahedra sharing faces with Si tetrahedra observed in Fe-bearing phase E exists in phase E' as well. The structures of Fe-bearing phase E and phase E', on the other hand, exhibit obvious differences in the stacking sequence of close-packed oxygen atoms, the distributions of M and Si cations between layers of close packed oxygen atoms, and the degree of the M cation ordering. The synthesis and characterization of Fe-bearing phase E and phase E' demonstrate that the phase E-type structures can be rather compliant and complex, and that as we further explore the temperature-pressure-composition space, other types of structures that are similar to or related to the structure of phase E may be discovered.

Introduction

Dense hydrous magnesium silicates (DHMS) synthesized at high temperatures and pressures have attracted much attention recently because of their potential role as major carriers for H and/or H_2O in the subducting slabs and the Earth's mantle. Ringwood and Major (1967) performed the first investigation on DHMS synthesized in the MgO-SiO_2-H_2O system in the temperature-pressure range of 10-18 GPa and 600-1100°C and identified three phases, designated by the letters A, B, and C. Since then, several other DHMS have been reported, including superhydrous phase C (Gasparik 1990), phase D (Yamamoto and Akimoto, 1977; Liu, 1986), phase E (Kanzaki, 1989, 1991), and phase G (Ohtani et al., 1997). While these DHMS have been widely studied structurally [see Prewitt and Parise (2000) for review], little is known about the effects of Fe on the crystal chemistry and stabilities of these phases, which is believed to be a major and important element in the mantle and which substitutes freely for Mg in a number of rock forming minerals (Hazen et al., 1992). In this study, we report the crystal structures of two Fe-bearing hydrous magnesium silicates synthesized at 1400°C and 14 GPa, one of which possesses the same structure ($R\bar{3}m$ symmetry) as phase E — a most unique and enigmatic class of high-pressure silicates in terms of crystal chemistry and thermodynamic stability (Kudoh et al., 1993). The other structure has the $P6_3/mmc$ symmetry and displays many features characteristic of phase E. Thus, we will call it phase E' hereafter for the simplicity of discussion.

The crystal structure of phase E consists of layers with brucite-type units cross-linked by Si in tetrahedral coordination, Mg in octahedral coordination, and hydrogen bonds (Kudoh et al., 1993). All three cation positions (Mg1, Mg2, and Si) are partially occupied; interlayer Mg octahedra and Si tetrahedra share edges and faces, respectively, with intralayer Mg octahedra. Because such a structural configuration is energetically unfavorable, Kudoh et al. (1993) proposed that interlayer cations in phase E are ordered locally in tens-of-angstroms-sized domains and there is no long-range order; all cations are distributed statistically throughout

H. Yang, yang@mail2.jpl.nasa.gov Corresponding author

an essentially close-packed arrangement of oxygen atoms. The ^{29}Si NMR spectroscopic measurement by Kanzaki et al. (1992) and Phillips et al. (1997) confirmed the occupation of all Si in tetrahedral coordination. The X-ray diffraction studies of phase E at high pressures (Shieh et al., 2000; Crichton and Ross, 2000) showed that phase E compresses nearly isotropically with the lowest bulk modulus (K_0 = 93 GPa) of all DHMS. The Raman and infrared spectra of phase E at ambient conditions and/or various temperatures and pressures were conducted by Ohtani et al. (1995), Liu et al. (1997), Mernagh and Liu (1998), Frost and Fei (1998), Shieh et al. (2000), and Kleppe et al. (2001).

Experiments

Both Fe-bearing phase E and phase E' samples used in this study were synthesized in one charge in a multi-anvil apparatus at 14 GPa and 1400°C for 47 hours. The starting composition was $Mg_5Fe^{3+}{}_2Si_2O_{12}$ plus some H_2O and was designed for the study of the stability of Fe-bearing wadsleyite. After the run, the Pt_{100} sample container was embedded in epoxy resin and ground to expose the center of the charge, in which at least three different phases were identified: light-gray hydrous wadsleyite, a blue phase (Fe-bearing phase E), and a brown phase (phase E'), all forming relatively isometric crystals with sizes up to ~70 μm in diameter for Fe-bearing phase E and phase E'. The compositions of different phases were determined with an electron microprobe (JEOL Superprobe). Pure SiO_2, MgO, and Fe_2O_3 were used as standards. Because the oxygen fugacity in a water-saturated experiment at the temperature and pressure of the present run was above the magnetite-hematite buffer, we thus assume that all iron in the charge is Fe^{3+}. The average compositions (n = 6) for the two studied samples are presented in Table 1. Given the results of the structural analysis, the chemical formulae were calculated on the basis of six oxygen atoms per unit cell by assuming that the difference from the total weight of 100% is ascribed to H_2O.

Based on optical examination, a nearly isometric crystal (~60 μm in diameter) was selected from each phase, Fe-bearing phase E and phase E'. Neither crystal, examined first with precession photography, showed any apparent diffuse scattering. They were then mounted on a Bruker Smart CCD X-ray diffractometer equipped with graphite-monochromatized MoK_α radiation (λ = 0.71069 Å). A hemisphere of three-dimensional X-ray diffraction data ($0° < 2\theta < 54°$) was collected for each sample with frame widths of 0.3° in ω and 30 s counting time per frame. The data were analyzed to locate peaks for determination of unit-cell parameters (Table 2). An empirical correction for X-ray absorption was made using the program SADABS (incorporated in SAINT). The detailed experimental procedures were similar to that described by Yang and Konzett (2000).

Examination of measured reflections suggested the possible space groups *R*32, *R*3*m*, or $R\bar{3}m$ for Fe-bearing phase E, and $P6_3mc$, $P\bar{6}2c$, or $P6_3/mmc$ for phase E'. Both structures were solved assuming the centric symmetry (i.e., $R\bar{3}m$ for Fe-bearing phase E and $P6_3/mmc$ for phase E') and refined using SHELX97. An attempt to refine the structures using non-centric symmetry did not produce significant improvement in the refinement statistics. The difference Fourier maps at the convergence of the refinements revealed no obvious peaks, and thus we were unable to locate the H positions. Both structures were refined with anisotropic atomic thermal displacement parameters. The low cation occupancy of Fe (0.06) at the M2 site of Fe-bearing phase E caused an instability of the atomic thermal displacement parameters for this atom during the refinements. Thus, the M1 and M2 cations were constrained to have the same atomic displacement parameters. The resulting R_1 and wR_2 factors for the two phases are given in Table 2. Final atomic coordinates and equivalent isotropic displacement parameters are presented in and selected bond distances in Table 4.

Synchrotron infrared absorption experiments were performed on a Bruker IFS 66s/V FTIR spectrometer at

Table 1. Chemical compositions for Fe-bearing phase E and phase E'

	Fe-bearing Phase E (blue)	Phase E' (brown)
MgO	42.85	41.34
Fe_2O_3	19.85	22.54
SiO_2	28.32	25.16
Total	91.02	89.04
Cation numbers per six oxygen atoms based on microprobe data		
Mg	2.22(1)	2.13(1)
Fe	0.52(1)	0.59(1)
Si	0.98(1)	0.87(1)
Cation numbers per six oxygen atoms based on X-ray refinement		
Mg	2.01(5)	2.22(8)
Fe	0.57(5)	0.63(8)
Si	1.03(1)	0.73(5)

Table 2. Crystal data for Fe-bearing phase E and phase E'

	a(Å)	*c*(Å)	V(Å^3)	S.G.	Observed Refl. [I > 2_(I)]	R_1 and R_w^2 factors	Reference
Phase E	2.9731(2)	13.9051(2)	106.45(3)	$R\bar{3}m$	43	0.028 and 0.022	Kudoh et al. (1993)
Fe-bearing Phase E	2.981(1)	13.898(3)	107.0(1)	$R\bar{3}m$	41	0.018 and 0.043	This study
Phase E'	2.953(1)	14.170(1)	107.0(1)	$P6_3/mmc$	58	0.026 and 0.071	This study

Note: R-factors reported by Kudoh et al. (1993) have different forms from those determined from the SHELX97 program.

the U2A beam line of National Synchrotron Light Source at Brookhaven National Laboratory. For comparison with Fe-bearing phase E and phase E', we also measured the IR spectrum for a phase E sample synthesized by Frost and Fei (1998). To avoid any saturated IR absorption, a diamond anvil cell was used to make thin film samples (~1 μm thick) by crushing single crystals, and transferring them from the anvil to a KBr substrate for further IR experiments. The aperture was set to 20 × 30 μm to ensure that only the spectra of samples were obtained. The spectra were collected with a nitrogen cooled MCT detector and a resolution of 4 cm^{-1} and 1024 scans was used for each sample and reference spectrum. The details of the synchrotron IR optical system have been given elsewhere (Liu et al. 2001).

Results and Discussion

The structure of phase E' possesses many features similar to that of Fe-bearing phase E. For example, they have similar chemical compositions (Table 1) and unit-cell parameters (Table 2). Most notably, both structures are built of close-packed oxygen atoms along the *c* axis, with all Si occupying the interstitial tetrahedral sites and M (= Mg + Fe) cations occupying the octahedral sites. All cation sites are partially occupied in both structures. The implausible configuration of M octahedra sharing faces with Si tetrahedra observed in Fe-bearing phase E exists in phase E' as well (Fig. 1). As pointed out by Kudoh et al. (1993), such a structure is unlikely to form at the experimental conditions (14 GPa and 1000°C), and the associated M cations must be absent in any unit cell in which Si is present. Because no super-lattice reflections or significant diffuse scattering was detected in the experiment, the coupled placement for M and Si cations must be randomly distributed in space.

The structures of Fe-bearing phase E and phase E', on the other hand, show some obvious differences. One of them is in the stacking sequence of close-packed oxygen atoms. In Fe-bearing phase E, oxygen atoms are stacked along the *c* dimension in a sequence of ABCABC in a unit cell, whereas they are stacked in a sequence of ABCBAC in phase E'. The distributions of cations between layers of close packed oxygen atoms also differ in the two structures, as illustrated in Fig. 2. In particular, there is only one type of Si tetrahedral site in Fe-bearing phase E and it is located between every *other* oxygen-atom layer. However, there are two crystallographically-distinct Si tetrahedral sites in phase E' and they are found between every oxygen-atom layer. Another noticeable structural dissimilarity between Fe-bearing phase E and phase E' is manifested in the degree of M cation ordering. In Fe-bearing phase E, the M cation, especially Mg, primarily occupies the M1 octahedral site, with M1 / M2 occupancy = 13.3. In contrast, the M cation, especially Mg, shows the preference for the M2 octahedral site over the M1 site in phase E', with M1 / M2 = 0.5 (Table 3). The dominant ordering of the M cation in the M1 site in Fe-bearing phase E is most likely to result from the fact that the M1 cations do not occupy the layers where the Si cations are present (Fig. 2), so the energetically-unfavorable configuration of the M octahedra sharing faces with the Si tetrahedra within the same layer can be avoided.

There could be many mechanisms for the substitution of a trivalent cation, R^{3+} (= Fe^{3+}, Al^{3+}, etc.), into a HDMS phase, but the following three or their combinations may be the most important and common:

(1) $2R^{3+} + \square \rightarrow 3Mg^{2+}$, where $\square$ stands for a vacancy;

(2) $R^{3+} + H^{+} \rightarrow Si^{4+}$;

(3) $2R^{3+} \rightarrow Mg^{2+} + Si^{4+}$;

Examination of previously published data on phase E shows that the Si content in our Fe-bearing phase E is very comparable to that in Fe-free phase E (about 1.0—1.2 per unit cell), indicating that mechanism (1) should dominate for the formation of Fe-bearing phase E. Due to the lack of data available for Fe-free phase E', however, it is difficult for us to draw a conclusion for phase E' in this regard.

Although the samples we used in this study were synthesized at pressures where some of the Si atoms might be expected to be in the octahedral coordination,

Table 3. Atomic coordinates and isotropic displacement factors for Fe-bearing phase E and phase E'.

Site			Fe-bearing Phase E ($R\bar{3}m$)	Phase E' ($P6_3/mmc$)
M1	Mg	occupancy	0.670(17)	0.012(14)
	Fe	occupancy	0.130(16)	0.284(11)
	x		0	0
	y		0	0
	z		0	0
	Ueq		0.018(1)	0.023(2)
M2	Mg	occupancy	0	0.544(17)
	Fe	occupancy	0.060(4)	0.016(15)
	x		1/3	1/3
	y		2/3	2/3
	z		1/6	0.3262(1)
	Ueq		0.018(1)	0.021(2)
Si1	Si	occupancy	0.172(5)	0.124(14)
	x		0	0
	y		0	0
	z		0.1280(3)	0.3748(4)
	Ueq		0.011(1)	0.017(5)
Si2	Si			0.058(12)
	x			1/3
	y			2/3
	z			0.4560(11)
	Ueq			0.027(9)
O1	x		0	0
	y		0	0
	z		0.2511(1)	1/4
	Ueq		0.029(1)	0.025(2)
O2	x			1/3
	y			2/3
	z			0.5849(2)
	Ueq			0.029(2)

our data show that all Si is tetrahedrally coordinated in both Fe-bearing phase E and phase E'. This observation is consistent with that obtained for Fe-free phase by Kudoh et al. (1993) from single-crystal X-ray diffraction and by Kanzaki et al. (1992) and Phillips et al. (1997) from the ^{29}Si NMR spectroscopic measurements.

Shieh et al. (2000) measured the compressibility of Fe-free phase E with the composition $Mg_{2.23}Si_{1.18}O_6H_{2.80}$ up to 14.5 GPa with synchrotron radiation and derived the bulk modulus K_0 = 94(2) GPa, with linear compressibilities $\beta_a = 4.23 \times 10^{-2}$ GPa^{-1} and $\beta_c = 5.14 \times 10^{-2}$ GPa^{-1}. Using single-crystal X-ray diffraction, Crichton and Ross (2000) determined the isothermal equation of state of a phase E crystal with the composition $Mg_{1.96}Fe_{0.07}Si_{1.04}O_6H_{3.7}$ up to 6.67 GPa and

Table 4. Selected bond distances for Fe-bearing phase E and phase E'

Fe-bearing Phase E ($R\bar{3}m$)		Phase E'	($P6_3/mmc$)
M1-O (x6)	2.066(1)	M1-O2 (x6)	2.087(2)
M2-O (x6)	2.083(1)	M2-O1 (x3)	2.018(1)
		M2-O2 (x3)	2.120(2)
Si-O (x1)	1.710(5)	Si1-O1 (x1)	1.768(5)
Si-O (x3)	1.835(2)	Si1-O2 (x3)	1.798(2)
		Si2-O2 (x1)	1.826(15)
		Si2-O2 (x3)	1.801(5)
M1-Si (x2)	1.779(4)	M1-Si1 (x2)	1.774(5)
M2-Si (x6)	1.803(1)	M1-Si2 (x6)	1.815(5)
		M2-Si1 (x3)	1.839(2)
		M2-Si2 (x1)	1.839(16)
Si-Si (x3)	2.029(4)	Si1-Si2	2.057(5)

reported K_0 = 93(1) GPa, with $\beta_a = 2.86 \times 10^{-3}$ GPa^{-1} and $\beta_c = 2.94 \times 10^{-3}$ GPa^{-1}. Although the bulk moduli given by the two groups of people are almost identical, the linear axial compressibilities are surprisingly discrepant, by nearly as much as an order of magnitude. These results are rather misleading, as the pressure dependencies of the unit-cell parameters [L = L (P)] given by Crichton and Ross (2000) are almost indistinguishable from those determined by Shieh et al. (2000). Using the given quadratic functions for the unit-cell parameters as a function of pressure, we have recalculated linear compressibilities of phase E based on the equation $\beta_L = -(1 / L_0)[\partial L(P) / \partial P]_{P=0}$ (Hazen and Finger 1982) and obtained $\beta_a = 3.71 \times 10^{-3}$ GPa^{-1} and $\beta_c = 3.89 \times 10^{-3}$ GPa^{-1} from the data of Shieh et al. (2000), and $\beta_a = 3.41 \times 10^{-3}$ GPa^{-1} and $\beta_c = 3.57 \times 10^{-3}$ GPa^{-1} from the data of Crichton and Ross (2000). The newly calculated linear axial compressibilities indicate that both *a* and *c* dimensions of phase E studied by Crichton and Ross (2000) are slightly less compressible than the corresponding dimensions of phase E examined by Shieh et al. (2000). However, it is unclear whether this slight dissimilarity in the axial compressibilities is due to the difference in the chemical compositions, as the phase E sample studied by Crichton and Ross (2000) contains a trace amount of Fe^{2+}.

Crichton and Ross (2000) compared the linear axial compressibilities of phase E with other layered structures and noted that phase E does not display apparent anisotropic compression ($\beta_c / \beta_a \approx 1.0$) as expected for layered structures, such as phase D, which has the highest bulk modulus among DHMS (Frost and

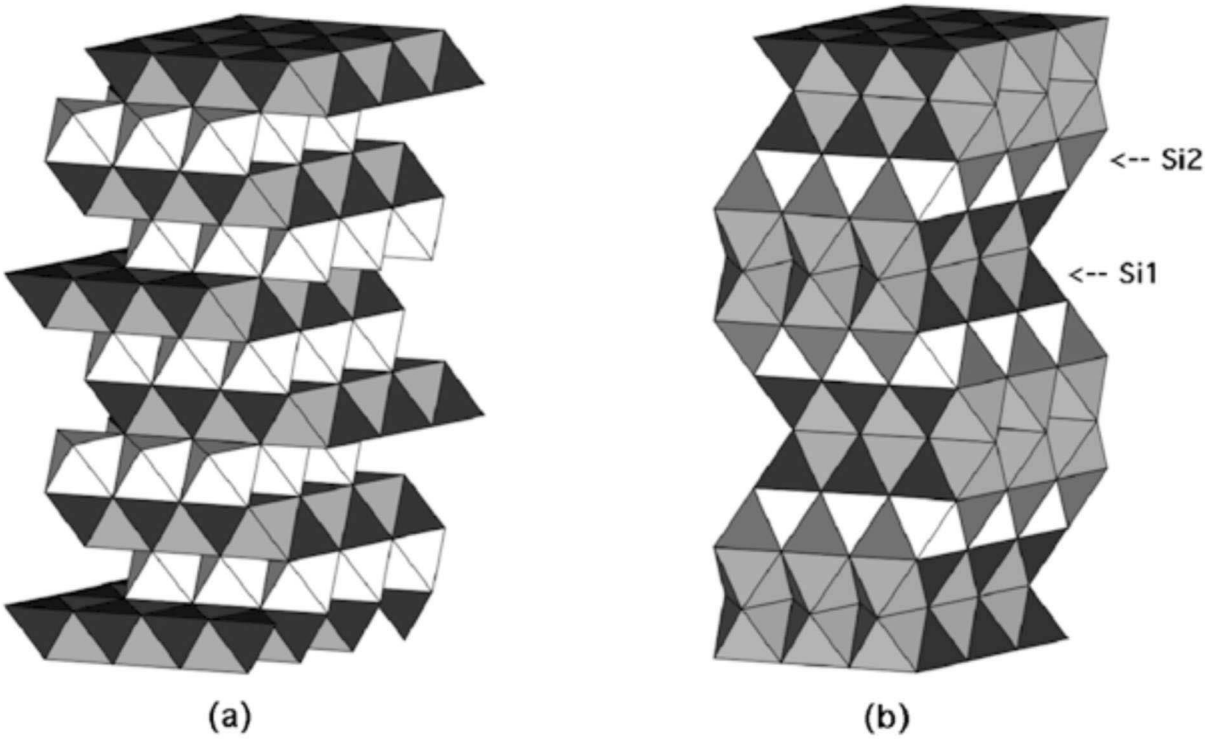

Figure 1. Comparison of crystal structures of (a) Fe-bearing phase E and (b) phase E'. The darkest triangles are faces of tetrahedra and the lighter ones are faces of octahedra.

Fei, 1998). They suggested that the introduction of interlayer Si and M polyhedra into the phase E structure serves to reduce both the compression anisotropy, by reducing the compressibility perpendicular to the sheets, and the ability to shear, by increasing the coherence between layers. Crichton and Ross (2000) also stated that, "even though several 'phase Es' may exist with and without Fe, there will be little difference in their compressibilities, given the comparability of our data to that previously determined by Shieh et al. (2000)." If this is the case, we should expect that phase E' exhibits an even less anisotropic compression and significantly larger shear modulus than phase E, as Si cations in phase E' exist between every close-packed oxygen-atom layers. Nevertheless, whether or not phase E' is less compressible than phase E will require further experimental determination.

Mernagh and Liu (1998) measured micro-Raman and micro-infrared spectra of the silicate and principal OH-stretching regions from a phase E specimen with the composition $Mg_{2.17}Si_{1.01}O_6H_{3.62}$ and found that the number of observed infrared and Raman bands exceeds the number predicted by factor-group analysis for a crystal of phase E with space group $R\bar{3}m$. This observation leads them to suspect that some long-range ordering or a superstructure may exist in phase E, such that it lowers the overall symmetry of the crystal, resulting in an increase in the number of vibrational bands in the spectra. These results appear to conflict with the selected-area electron diffraction (SAED) patterns obtained by Kudoh et al. (1993), which do not reveal the existence of any long-range superstructure. Mernagh and Liu (1998) argued that the interpretation presented by Kudoh et al. (1993) was based solely on the similarities between the diffuse scattering in the

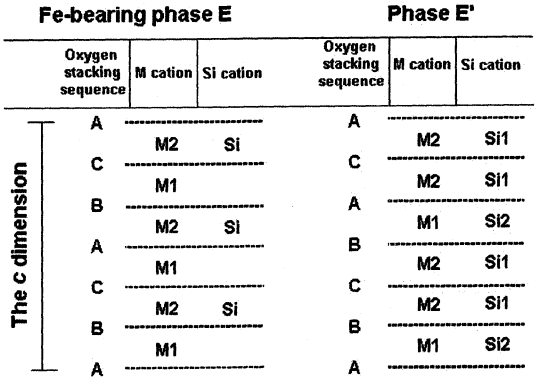

Figure 2. Illustration of atomic stacking sequences and arrangements for Fe-bearing phase E and phase E'.

SAED and that observed in short-range-ordered alloys.

Plotted in Figure 3 are the infrared absorption spectra we measured for phase E, Fe-bearing phase E, and E'. The similarities among them are evident, as expected from the similarities in the structures of these phases. There are two very broad bands between 3000 and 3700 cm^{-1} with tails toward the low frequency and three intense bands below 1000 cm^{-1} for all samples. The broad bands in the principal OH-stretching region are due to either H_2O or weakly bonded OH, or both, indicating that the hydrogen atoms could be highly delocalized. The intense bands observed below 1000 cm^{-1} are attributed to Si-O stretching vibrations of the isolated SiO_4 tetrahedra (Mernagh and Liu, 1998). It is interesting to note that there is a systematic shift for all bands below 1000 cm^{-1} toward lower frequency from phase E to phase E', except for the lowest frequency mode around 800 cm^{-1}. This band shift could be related to the increase in the average Si-O bond distance from phase E to phase E', as seen in Table 4. In addition, the bands below 1000 cm^{-1} become increasingly more overlapped from phase E to phase E'. This observation is possibly associated with the substitution of Fe^{3+} for Mg^{2+} and the different structural symmetry, which is higher for phase E' than for phase E.

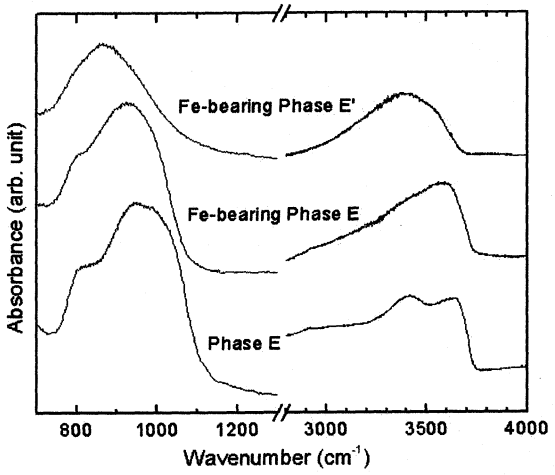

Figure 3. Synchrotron IR absorption spectra of phase E, Fe-bearing phase E and phase E'.

Conclusions

The synthesis and characterization of Fe-bearing phase E and phase E' show that the phase E-type structures can be rather compliant and complex, and are capable of incorporating a variety of cations with different sizes and valences. Our study also implies that, as we further explore the temperature-pressure-composition space, other types of structures that are similar to or related to the structure of phase E may be discovered. It would be interesting to extend similar investigations into other DHMS as well. Furthermore, this study reaffirms the necessity of more systematic studies by combining structure determination/refinements with spectroscopic measurements for our better understanding of crystal chemistry of high-pressure phases in general and DHMS in particular. Regardless of these, some questions remain to be addressed. One of them is to what extent the phase E-type structures can allow the substitution of Fe for Mg. Another question is about the stability of phase E, which was thought to be thermodynamically metastable by Kudoh et al. (1993). From the high-pressure X-ray diffraction measurement, Shieh et al. (2000) concluded that the disorder structure of phase E is not a result of pressure quenching, but they did not rule out the possibility of its formation resulting from temperature quenching. The mystery about the disorder structure and stability of phase E may remain until in-situ high-temperature and high-pressure data on this phase become available.

Acknowledgements

We thank Dr. Y. Fei at the Geophysical Laboratory for providing us with the samples used in this study. Comments for the improvement of the manuscript by Dr. M. Matsui and an anonymous reviewer are appreciated. The work described in this paper was performed at the Geophysical Laboratory and supported by NSF grant EAR-9973018 and the Center for High Pressure Research. The writing and publication of this paper was supported by the Jet Propulsion Laboratory, California Institute of Technology, under a contract with the National Aeronautics and Space Administration. Reference herein to any specific commercial product, process, or service by trade name, trademark, manufacturer, or otherwise, does not constitute or imply its endorsement by the United States Government or the Jet Propulsion Laboratory, California Institute of Technology.

References

Crichton, W.A. and Ross, N.L. (2000) Equation of state of phase E. Mineralogical Magazine, 64, 561-567.

Frost, D.J. and Fei, Y. (1998) Stability of phase D at high pressure and high temperature. Journal of Geophysical Research, 103, 7463-7474.

Gasparik, T. (1990) Phase relations in the transition zone. Journal of Geophysical Research, 95, 15751-15769.

Hazen, R.M. and Finger, L.W. (1982) Comparative Crystal Chemistry. Wiley, New York.

Hazen, R.M., Finger, L.W., and Ko, J. (1992) Crystal chemistry of Fe-bearing anhydrous phase B: Implications for transition zone mineralogy. American Mineralogist, 77, 217-220.

Kanzaki, M. (1989) High pressure phase relations in the system MgO-SiO_2-H_2O. EOS, 70, 508.

Kanzaki, M. (1991) Stability of hydrous magnesium silicates in the mantle transition zone. Physics of the Earth and Planetary Interiors, 66, 307-312.

Kanzaki, M., Stebbins, J.F., and Xue, X. (1992) Characterization of crystalline and amorphous silicates quenched from high pressure by ^{29}Si MAS NMR spectrocscopy. In Syono Y, Manghnani MH (eds): High-pressure research: Application to Earth and Planetary Sciences. American Geophysical Union, Washington, D.C., pp 89-100.

Kleppe, A.K., Jephcoat, A.P., and Ross, N.L. (2001) Raman Spectroscopic studies of phase E to 19 GPa. American Mineralogist, 86, 1275-1281.

Kudoh, Y., Finger, L.W., Hazen, R.M., Prewitt, C.T., Kanzaki, M., and Veblen, D.R. (1993) Phase E: A high pressure hydrous silicate with unique crystal chemistry. Physics and Chemistry of Minerals, 19, 357-360.

Liu, L.G. (1986) Phase transformations in serpentine at high pressures and temperatures and implications for subducting lithosphere. Physics of the Earth and Planetary Interiors, 42, 255-262.

Liu, L.G., Mernagh, T.P., Lin, C.C., and Irifune, T. (1997) Raman spectra of phase E at various pressures and temperatures with geophysical implications. Earth and Planetary Science Letters, 149, 57-65.

Liu, Z., Hu, J., Yang, H., Mao, H.K., and Hemley, R.J. (2001) High-pressure synchrotron x-ray diffraction and infrared microspectrascopy: applications to dense hydrous phases. Proceedings of the 18th International Conference on High Pressure Science and Technology (in press).

Mernagh T.P. and Liu, L.G. (1998) Raman and infrared spectra of phase E, a plausible hydrous phase in the mantle. Canadian Mineralogist, 36, 1217-1223.

Ohtani, E., Shibata, T., Kubo, T., and Kato, T. (1995) Stability of hydrous phases in the transition zone and the upper most part of the lower mantle. Geophysical Research Letters, 22, 2553-2556.

Ohtani, E., Mizobata, H., Kudoh, Y., Nagase, T., Arashi, H., Yurimoto, H., and Miyagi, I. (1997) A new hydrous silicate, a water reservoir, in the upper part of the lower mantle. Geophysical Research Letters, 24, 1047-1050.

Phillips, B.L., Burnley, P.C., and Worminghaus, K. (1997) ^{29}Si and ^{1}H NMR spectroscopy of high-pressure hydrous magnesium silicates. Physics and Chemistry of Minerals, 24, 179-190.

Prewitt, C.T. and Parise, J.B. (2000) Hydrous phases and hydrogen bonding at high pressure. Reviews in Mineralogy and Geochemistry, vol. 41, 309-333.

Ringwood, A.E., and Major, A. (1967) High pressure reconnaissance investigations in the system Mg_2SiO_4-MgO-H_2O. Earth and Planetary Science Letters, 2, 130-133.

Shieh, S.R., Mao, H.K., Konzett, J., and Hemley, R.J. (2000) In-situ high pressure X-ray diffraction of phase E to 15 GPa. American Mineralogist, 85, 765-769.

Yamamoto, K. and Akimoto, S. (1977) The system MgO-SiO_2-H_2O at high pressures and temperatures-stability field for hydroxyl-chondrodite, hydroxyl-clinohumite, and 10 Å-phase. American Journal of Science, 277, 288-312.

Yang, H. and Konzett, J. (2000) High-pressure synthesis of $Na_2Mg_6Si_6O_{18}(OH)_2$—a new hydrous silicate phase isostructural with aenigmatite. American Mineralogist, 85, 259-262.

Manuscript received; 29 March, 2002
Manuscript accepted; 18 June, 20002